Science Advances
AAAS

Supplementary Materials for

Differences in ion-RNA binding modes due to charge density variations explain the stability of RNA in monovalent salts

Anja Henning-Knechtel *et al*.

Corresponding author: D. Thirumalai, dave.thirumalai@gmail.com; Serdal Kirmizialtin, serdal@nyu.edu

Sci. Adv. **8**, eabo1190 (2022)
DOI: 10.1126/sciadv.abo1190

This PDF file includes:

Section S1

General Setting for Molecular Dynamic Simulations.

We added explicit water and ions to neutralize the RNA charge, and to mimic the experimental concentration of 400 mM monovalent salt. We created two systems, one RNA in NaCl aqueous solution and the other is in KCl with the same ionic strength. We kept the number of atoms constant in each simulation to allow direct comparison of the extensive properties of RNA in Na^+ and K^+. We added 771 Cl^- and 822 (Na^+/K^+) to the simulation boxes by replacing some of the water molecules. We used ff99paramsbc0 force field to represent the RNA,[52] Smith and Dang parameters[59] for ions, and TIP3P[60] for water.

The energy of the solvated systems were minimized for about 5000 MD steps using the steepest descent method. This process eliminated high energy contacts that may arise due to random placement of water and ions. The minimized structures were then equilibrated as explained below.

First, we employed a 2.5-ns long simulation in isothermal – isobaric ensemble (NPT) by keeping the temperature at 300 K using the Berendsen thermostat.[61] Parrinello-Rahman barostat[62] was used to maintain the pressure at 1 bar. The heavy atoms of the RNA were restrained to their initial positions using harmonic restraints with a force constant of 1000 kJ/nm^2 while ions and water were allowed to move freely. Periodic boundary conditions were implemented in the three directions. Particle Mesh Ewald (PME) summation[63] was used to compute long-range electrostatic interactions. The real space distance cutoff (for electrostatics and van der Waals energies) was set to 11Å. The grid for the Fourier space summation in the PME was 1.6Å, and fourth order splines were used to interpolate the charge density on the grid. A dispersion correction was made for the van der Waals cutoff. Covalent bonds in the water and RNA were constrained to their equilibrium geometries using SETTLE[64] and LINCS[65] algorithms, respectively. The equations of motion were integrated using the Leap-Frog scheme with a time step of 1 fs.

The dimensions and the positions of atoms at the last snapshot of the NPT simulation were saved and used to initiate the solvent equilibration step. This procedure ensures that ions and water molecules reach equilibrium before the production runs. For this purpose, we used a further restrained, 60-ns long NVT run keeping all the settings from the previous section the same except the barostats were turned, off and Velocity scaling was employed.[66]

Supplementary Figures and Analysis

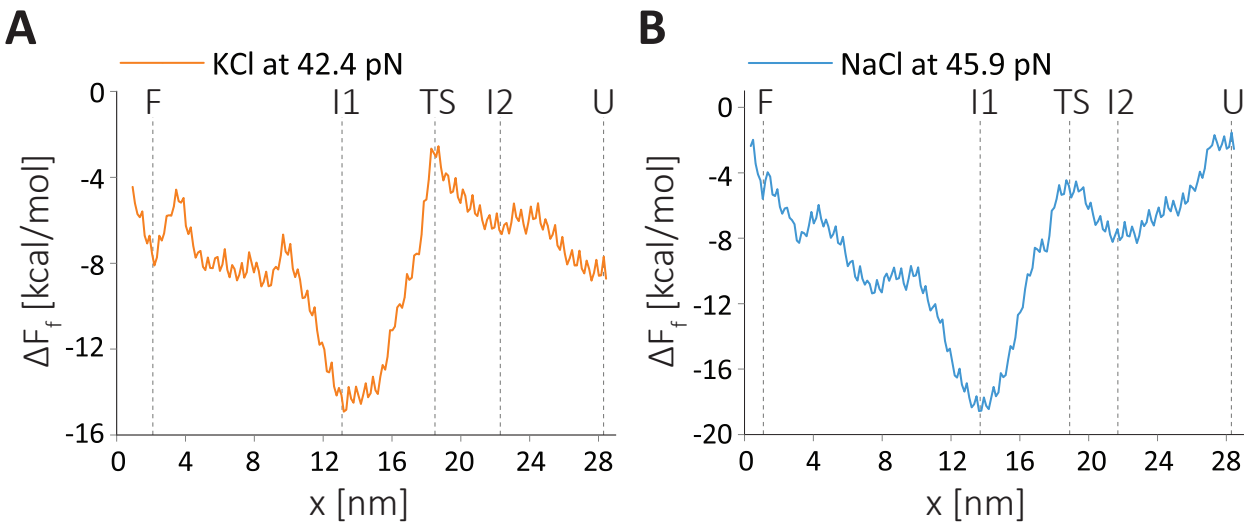

Figure S1: Free energy at the unfolding transition where folded and unfolded populations of RNA are equal. The effect of force (f) on the landscape F_f is given as $F_f(x) = F_0(x) - fx$, with x the displacement along the pulling direction. (A) is for K^+, and (B) is for Na^+. Major intermediate states are represented by vertical lines that explained in Fig. 2. The minimum at the midpoint force corresponds to $I1$ state where additional stabilization occurs due to non-native contact formation explained in Figure S2.

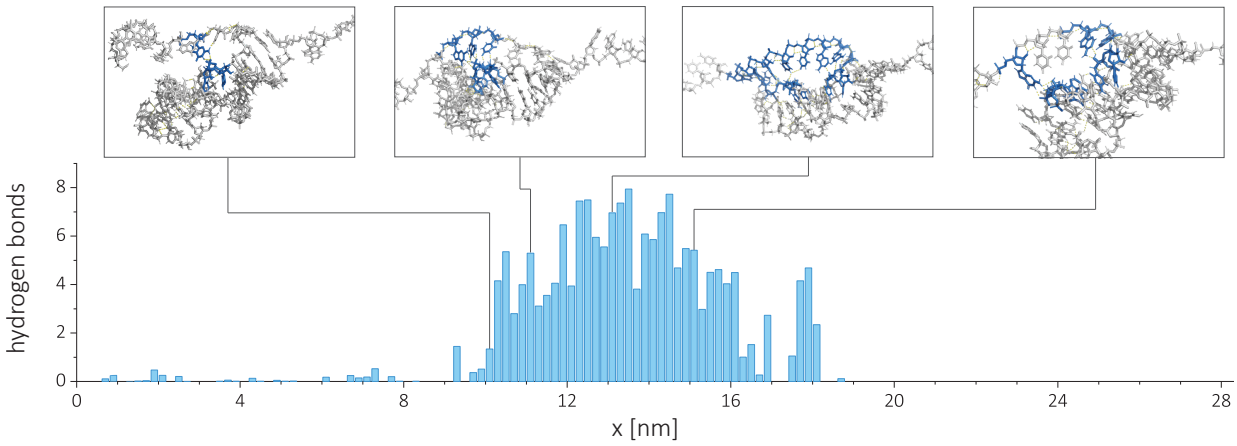

Figure S2: Average number of inter-residue hydrogen bond formation as a function of extension for HIV-1 TAR hairpin in NaCl. The average number of hydrogen bonds were computed between segments 6U-14C and 21U-37C. Insets show representative structures at $x \approx$10.1, 11.1, 13.1, and 15.1 nm. The residues that form hydrogen bonds are highlighted in blue. Similar results obtained for RNA in KCl

Conformational entropy and radius of gyration analysis. To elucidate the mechanism of cation size on RNA stability we compute the conformational entropy and the degree of compaction as a function of extension. As the RNA unfolds the conformational entropy increases (Fig. S3A). A linear increase in the entropy between $x \approx (0-9nm)$ coincides with the unzipping of the extended stem region. Interestingly, unzipping in the range $x \approx (9-16\ nm)$ results in a smaller change in entropy because it involves disruption of 3-nt apical loop region, which is structurally already disordered even in the folded state. The rupture of the base pair 36U-18A (Inset in Fig. 2A-B) results in an abrupt increase in entropy. The rupture coincides well with the transition state location (Fig. 2A-B). After the transition state, the entropy change shows a linear increase with extension.

The change in the radius of gyration (R_g) of RNA on the other hand, is impervious to increase in the extension at $x \approx (0-8\ nm)$, as is evident from the nearly flat region in Fig. S3(B). After the rupture of the lower stem (Fig. 2A-B) the R_g ramps up. However, neither entropy, nor radius of gyration show cation size related differences.

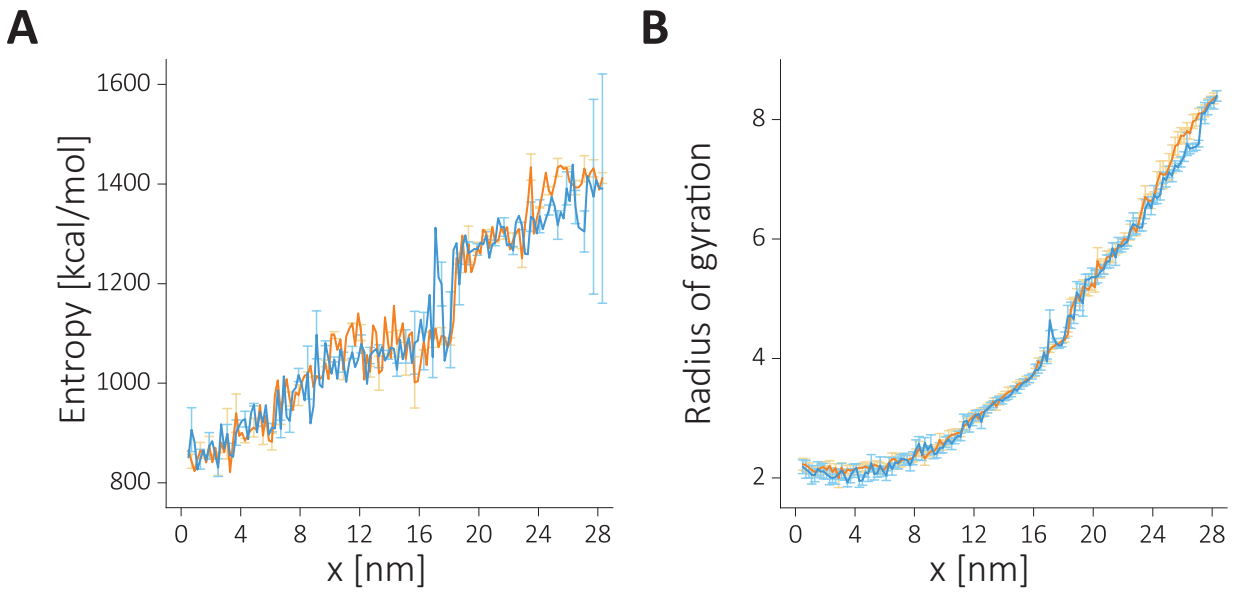

Figure S3: The change in the RNA conformational entropy and RNA compaction as RNA undergoes unfolding transition with applied force. The RNA in the presence of KCl (orange) or in NaCl (blue). A) The change in the RNA conformational entropy in (TS) as a function of extension. B) The change in the radius of gyration during the unfolding process.

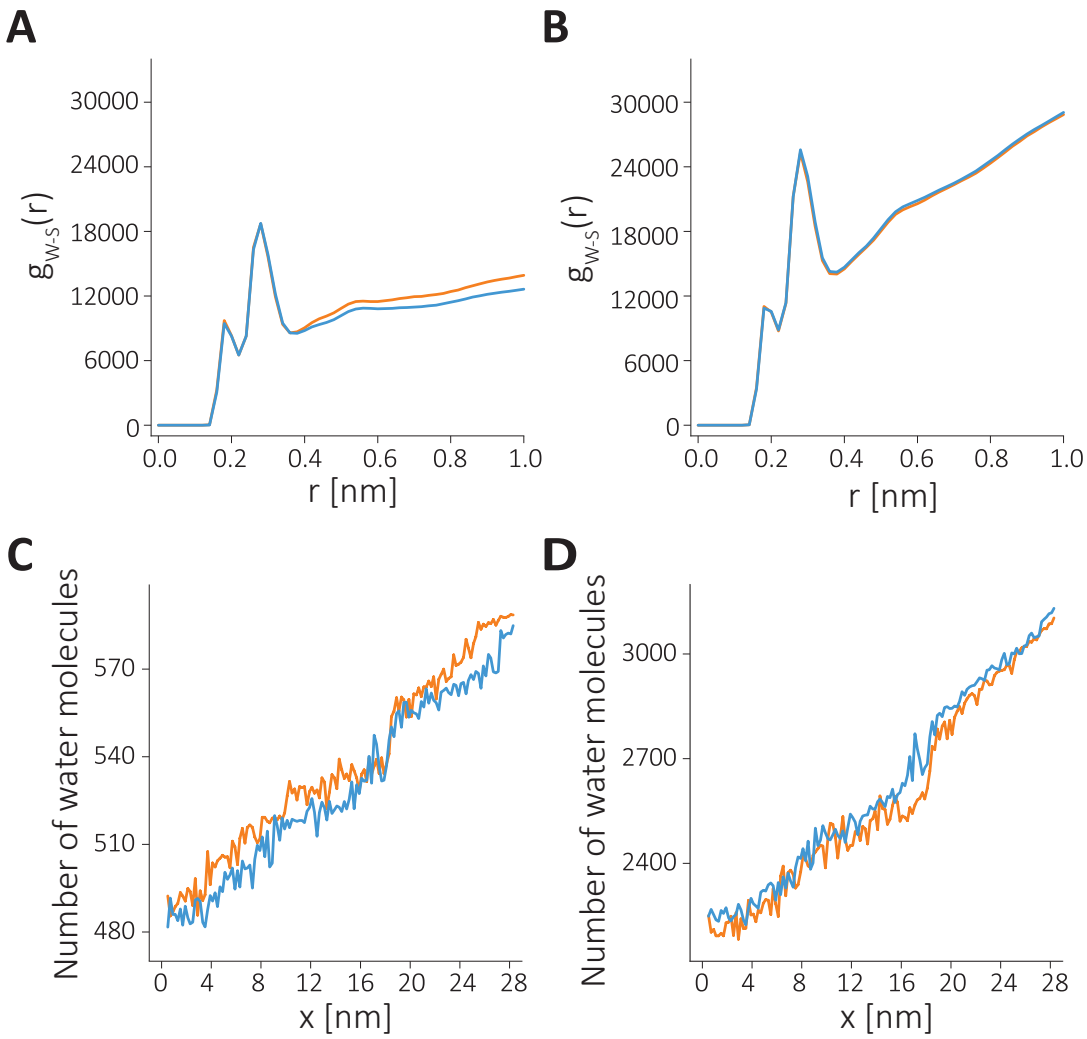

Figure S4: Radial distribution function (RDF) of water molecules around the surface of HIV-1 TAR hairpin at the folded and unfolded states. Data for Na^+ and K^+ are given in blue and orange, respectively. A-B) RDF of water (W) with the RNA surface (s) at the folded and at the unfolded states respectively. (C-D) Changes in the cumulative number of water molecules around RNA as a function of extension. The number of surface-bound water molecules was calculated based on equation 1. C) Directly binding water coordination (set by cut-off: 0.22 nm) and, D) in directly binding water coordination (cut-off: 0.36 nm).

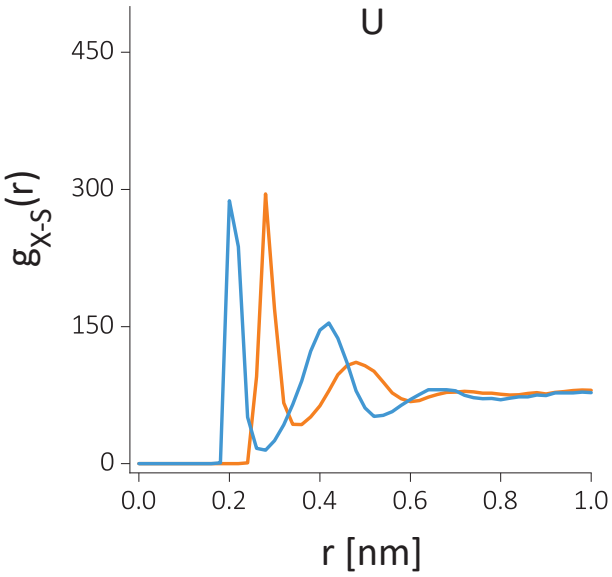

Figure S5: Radial distribution function (RDF) of cation–RNA, $g_{X-S}(r)$, for the unfolded state U.

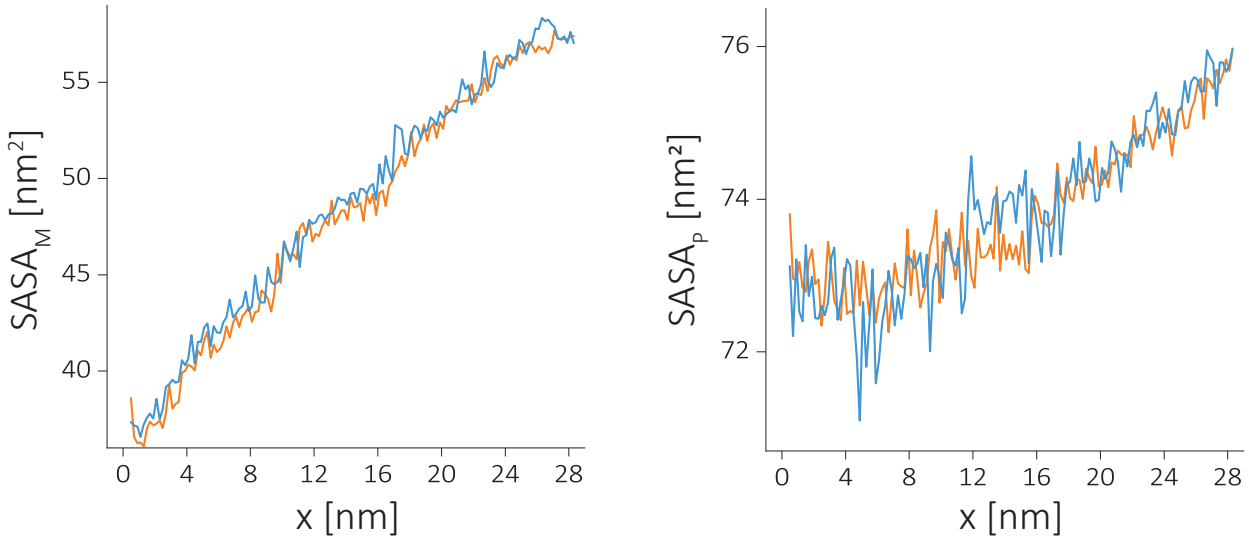

Figure S6: Solvent accessible surface area (SASA) computed along the unfolding pathway. A) SASA of the major grooves and, B) SASA of the phosphate groups. Na^+ (blue) and K^+ (orange)

REFERENCES AND NOTES

1. S. A. Woodson, Metal ions and RNA folding: A highly charged topic with a dynamic future. *Curr. Opin. Chem. Biol.***9**, 104–109 (2005).

2. D. Thirumalai, C. Hyeon, RNA and protein folding: Common themes and variations *Biochemistry* **44**, 4957–4970 (2005).

3. M. Wu, I. Tinoco Jr., RNA folding causes secondary structure rearrangement. *Proc. Natl. Acad. Sci. U.S.A.* **95**, 11555–11560 (1998).

4. D. Thirumalai, Native secondary structure formation in RNA may be a slave to tertiary folding. *Proc. Natl. Acad. Sci. U.S.A.* **95**, 11506–11508 (1998).

5. E. Koculi, S. S. Cho, R. Desai, D. Thirumalai, S. A. Woodson, Folding path of P5abc RNA involves direct coupling of secondary and tertiary structures. *Nucleic Acids Res.* **40**, 8011–8020 (2012).

6. R. Russell, I. S. Millett, S. Doniach, D. Herschlag, Small angle x-ray scattering reveals a compact intermediate in RNA folding. *Nat. Struct. Biol.* **7**, 367–370 (2000).

7. R. Russell, I. S. Millett, M. W. Tate, L. W. Kwok, B. Nakatani, S. M. Gruner, S. G. J. Mochrie, V. Pande, S. Doniach, D. Herschlag, L. Pollack Rapid compaction during RNA folding. *Proc. Natl. Acad. Sci. U.S.A.* **99**, 4266–4271 (2002).

8. K. Takamoto, R. Das, Q. He, S. Doniach, M. Brenowitz, D. Herschlag, M. R. Chance Principles of RNA compaction: Insights from the equilibrium folding pathway of the P4-P6 RNA domain in monovalent cations. *J. Mol. Biol.* **343**, 1195–1206 (2004).

9. I. Shcherbakova, S. Gupta, M. R. Chance, M. Brenowitz Monovalent ion-mediated folding of the tetrahymena thermophila ribozyme. *J. Mol. Biol.* **342**, 1431–1442 (2004).

10. G. Caliskan, C. Hyeon, U. Perez-Salas, R. M. Briber, S. A. Woodson, D. Thirumalai Persistence length changes dramatically as RNA folds. *Phys. Rev. Lett.* **95**, 268303 (2005).

11. A. Gopal, Z. H. Zhou, C. M. Knobler, W. M. Gelbart Visualizing large RNA molecules in solution. *RNA* **18**, 284–299 (2012).

12. K. A. Leamy, N. H. Yennawar, P. C. Bevilacqua Cooperative RNA folding under cellular conditions arises from both tertiary structure stabilization and secondary structure destabilization. *Biochemistry* **56**, 3422–3433 (2017).

13. G. S. Manning, Limiting laws and counterion condensation in polyelectrolyte solutions I. Colligative properties. *J. Chem. Phys.* **51**, 924–933 (1969).

14. G. S. Manning, Limiting laws and counterion condensation in polyelectrolyte solutions: IV. The approach to the limit and the extraordinary stability of the charge fraction. *Biophys. Chem.* **7**, 95–102 (1977).

15. G. S. Manning, The molecular theory of polyelectrolyte solutions with applications to the electrostatic properties of polynucleotides. *Q. Rev. Biophys.* **11**, 179–246 (1978).

16. F. Oosawa, *Polyelectrolytes* (Marcel Dekker, 1971).

17. D. E. Draper, A guide to ions and RNA structure. *RNA* **10**, 335–343 (2004).

18. E. Westhof, P. Dumas, D. Moras Restrained refinement of two crystalline forms of yeast aspartic acid and phenylalanine transfer RNA crystals. *Acta Crystallogr.* **44**, 112–124 (1988).

19. W. Scott, J. B. Murray, J. R. Arnold, B. L. Stoddard, A. Klug, Capturing the structure of a catalytic RNA intermediate: The hammerhead ribozyme. *Science* **274**, 2065–2069 (1996).

20. Y. Endo, A. Glück, I. G. Wool Ribosomal RNA identity elements for ricin A-chain recognition and catalysis. *J. Mol. Biol.* **221**, 193–207 (1991).

21. F. Jiang, R. A. Kumar, R. A. Jones, D. J. Patel Structural basis of RNA folding and recognition in an AMP–RNA aptamer complex. *Nature* **382**, 183–186 (1996).

22. E. Koculi, D. Thirumalai, S. A. Woodson Counterion charge density determines the position and plasticity of RNA folding transition states. *J. Mol. Biol.* **359**, 446–454 (2006).

23. N. Hori, N. A. Denesyuk, D. Thirumalai Ion condensation onto ribozyme is site specific and fold dependent. *Biophys. J.* **116**, 2400–2410 (2019).

24. A. Wang, M. Levi, U. Mohanty, P. C. Whitford, Diffuse ions coordinate dynamics in a ribonucleoprotein assembly. *J. Am. Chem. Soc.* **144**, 9510–9522 (2022).

25. A. P. Williams, C. E. Longfellow, S. M. Freier, R. Kierzek, D. H. Turner Laser temperature-jump, spectroscopic, and thermodynamic study of salt effects on duplex formation by dGCATGC. *Biochemistry* **28**, 4283–4291 (1989).

26. D. Lambert, D. Leipply, R. Shiman, D. E. Draper The influence of monovalent cation size on the stability of RNA tertiary structures. *J. Mol. Biol.* **390**, 791–804 (2009).

27. E. Koculi, C. Hyeon, D. Thirumalai, S. A. Woodson Charge density of divalent metal cations determines RNA stability. *J. Am. Chem. Soc.* **129**, 2676–2682 (2007).

28. S. L. Heilman-Miller, J. Pan, D. Thirumalai, S. A. Woodson Role of counterion condensation in folding of the Tetrahymena ribozyme. II. Counterion-dependence of folding kinetics. *J. Mol. Biol.* **309**, 57–68 (2001).

29. S. L. Heilman-Miller, D. Thirumalai, S. A. Woodson Role of counterion condensation in folding of the *Tetrahymena* ribozyme. I. Equilibrium stabilization by cations. *J. Mol. Biol.* **306**, 1157–1166 (2001).

30. M. L. Bleam, C. F. Anderson, M. T. Record Jr. Relative binding affinities of monovalent cations for double-stranded DNA. *Proc. Natl. Acad. Sci. U.S.A.* **77**, 3085–3089 (1980).

31. E. Stellwagen, N. C. Stellwagen, Probing the electrostatic shielding of DNA with capillary electrophoresis. *Biophys. J.* **84**, 1855–1866 (2003).

32. A. A. Zinchenko, K. Yoshikawa, Na^+ shows a markedly higher potential than K^+ in DNA compaction in a crowded environment. *Biophys. J.* **88**, 4118–4123 (2005).

33. N. Bisaria, D. Herschlag, Probing the kinetic and thermodynamic consequences of the tetraloop/tetraloop receptor monovalent ion-binding site in P4–P6 RNA by smFRET. *Biochem. Soc. Trans.* **43**, 172–178 (2015).

34. J. Vieregg, W. Cheng, C. Bustamante, I. Tinoco Measurement of the effect of monovalent cations on RNA hairpin stability. *J. Am. Chem. Soc.* **129**, 14966–14973 (2007).

35. J. Liphardt, B. Onoa, S. B. Smith, I. Tinoco Jr., C. Bustamante Reversible unfolding of single RNA molecules by mechanical force. *Science* **292**, 733–737 (2001).

36. P. T. X. Li, C. Bustamante, I. Tinoco Jr Real-time control of the energy landscape by force directs the folding of RNA molecules. *Proc. Natl. Acad. Sci.* **104**, 7039–7044 (2007).

37. J.-D. Wen, M. Manosas, P. T. X. Li, S. B. Smith, C. Bustamante, F. Ritort, I. Tinoco Jr. Force unfolding kinetics of RNA using optical tweezers. I. Effects of experimental variables on measured results. *Biophys. J.* **92**, 2996–3009 (2007).

38. F. S. Papini, M. Seifert, D. Dulin High-yield fabrication of DNA and RNA constructs for single molecule force and torque spectroscopy experiments. *Nucleic Acids Res.* **47**, e144 (2019).

39. R. Walder, W. J. van Patten, D. B. Ritchie, R. K. Montange, T. W. Miller, M. T. Woodside, T. T. Perkins High-precision single-molecule characterization of the folding of an HIV RNA hairpin by atomic force microscopy. *Nano Lett.* **18**, 6318–6325 (2018).

40. J. R. Vieregg, I. Tinoco, Modelling RNA folding under mechanical tension. *Mol. Phys.* **104**, 1343–1352 (2006).

41. Y.-Z. Shi, L. Jin, F. H. Wang, X. L. Zhu, Z. J. Tan Predicting 3D structure, flexibility, and stability of RNA hairpins in monovalent and divalent ion solutions. *Biophys. J.* **109**, 2654–2665 (2015).

42. A. Savelyev, G. A. Papoian, Electrostatic, steric, and hydration interactions favor Na^+ condensation around DNA compared with K^+. *J. Am. Chem. Soc.* **128**, 14506–14518 (2006).

43. G. M. Torrie, J. P. Valleau, Monte Carlo free energy estimates using non-Boltzmann sampling: Application to the sub-critical Lennard-Jones fluid. *Chem. Phys. Lett.* **28**, 578–581 (1974).

44. S. Kirmizialtin, L. Huang, D. E. Makarov Topography of the free-energy landscape probed via mechanical unfolding of proteins. *J. Chem. Phys.* **122**, 234915 (2005).

45. C. Hyeon, D. Thirumalai, Mechanical unfolding of RNA: From hairpins to structures with internal multiloops. *Biophys. J.* **92**, 731–743 (2007).

46. C. Hyeon, D. Thirumalai, Multiple probes are required to explore and control the rugged energy landscape of RNA hairpins. *J. Am. Chem. Soc.* **130**, 1538–1539 (2008).

47. M. Gebala, S. Bonilla, N. Bisaria, D. Herschlag Does cation size affect occupancy and electrostatic screening of the nucleic acid ion atmosphere? *J. Am. Chem. Soc.* **138**, 10925–10934 (2016).

48. W. He, S. Kirmizialtin, Exploring cation mediated DNA interactions using computer simulations, in *Advances in Bionanomaterials II* (Springer International Publishing, 2020), pp. 51–63.

49. A. Srivastava, R. Timsina, S. Heo, S. W. Dewage, S. Kirmizialtin, X. Qiu Structure-guided DNA–DNA attraction mediated by divalent cations. *Nucleic Acids Res.*. **48**, 7018**–**7026 2020.

50. F. Aboul-ela, J. Karn, G. Varani, Structure of HIV-1 TAR RNA in the absence of ligands reveals a novel conformation of the trinucleotide bulge. *Nucleic Acids Res.* **24**, 3974–3981 1996.

51. T. J. Macke, D. A. Case, Modeling unusual nucleic acid structures. *Am. Chem. Soc.*, **682**, 379–393 1997.

52. A. Pérez I. Marchán, D. Svozil, J. Sponer, T. E. Cheatham III, C. A. Laughton, M. Orozco, Refinement of the AMBER force field for nucleic acids: Improving the description of α/γ conformers. *Biophys. J.* **92**, 3817–3829 2007.

53. F. Musiani, G. Rossetti, L. Capece, T. M. Gerger, C. Micheletti, G. Varani, P. Carloni Molecular dynamics simulations identify time scale of conformational changes responsible for conformational

selection in molecular recognition of HIV-1 transactivation responsive RNA. *J. Am. Chem. Soc.*, **136**, 15631–15637 2014.

54. D. Kosztin, S. Izrailev, K. Schulten, Unbinding of retinoic acid from its receptor studied by steered molecular dynamics. *Biophys. J.* **76**, 188–197 1999.

55. S. Kumar, J. M. Rosenberg, D. Bouzida, R. H. Swendsen, P. A. Kollman The weighted histogram analysis method for free-energy calculations on biomolecules. I. The method. *J. Comput. Chem.* **13**, 1011–1021 1992.

56. J. S. Hub, B. L. de Groot, D. van der Spoel g_wham—A free weighted histogram analysis implementation including robust error and autocorrelation estimates. *J. Chem. Theory Comput.* **6**, 3713–3720 2010.

57. J. Schlitter, Estimation of absolute and relative entropies of macromolecules using the covariance matrix. *Chem. Phys. Lett.* **215**, 617–621 1993,.

58. H. T. Nguyen, D. Thirumalai, Charge density of cation determines inner versus outer shell coordination to phosphate in RNA. *J. Phys. Chem. B.* **124**, 4114–4122 2020.

59. D. E. Smith, L. X. Dang, Computer simulations of NaCl association in polarizable water. *J. Chem. Phys.* **100**, 3757–3766 1994.

60. W. L. Jorgensen, J. Chandrasekhar, J. D. Madura, R. W. Impey, M. L. Klein, Comparison of simple potential functions for simulating liquid water. *J. Chem. Phys.* **79**, 926–935 1983.

61. H. J. C. Berendsen, J. P. M. Postma, W. F. van Gunsteren, A. DiNola, J. R. Haak, Molecular dynamics with coupling to an external bath. *J. Chem. Phys.*, **81**, 3684–3690 1984.

62. M. Parrinello, A. Rahman, Polymorphic transitions in single crystals: A new molecular dynamics method. *J. Appl. Phys.* **52**, 7182–7190 1981.

63. T. Darden, D. York, L. Pedersen, Particle mesh Ewald: An $N\cdot\log(N)$ method for Ewald sums in large systems. *J. Chem. Phys.* **98**, 10089–10092 1993.

64. S. Miyamoto, P. A. Kollman, Settle: An analytical version of the SHAKE and RATTLE algorithm for rigid water models. *J. Comput. Chem.* **13**, 952–962 1992.

65. B. Hess, H. Bekker, H. J. C. Berendsen, J. G. E. M. Fraaije, LINCS: A linear constraint solver for molecular simulations. *J. Comput. Chem.* **18**, 1463–1472 1997.

66. G. Bussi, D. Donadio, M. Parrinello, Canonical sampling through velocity rescaling. *J. Chem. Phys.* **126**, 014101 2007.